11th International Conference on Electrical, Electronics and Computer Engineering (IcETRAN), Nis, 3-6 June 2024

Enhancing People Tracking in Frequency-Modulated Continuous-Wave Radar Systems: Optimal Parameter Selection for Integrated Probabilistic Data Association Filter Tracker

1st Milan Stojanovic
School of Electrical Engineering
University of Belgrade
Belgrade, Serbia
0000-0002-1783-1615

2nd Aleksa Jovanovic
Novelic Radar Sensors
Novelic
Belgrade, Serbia
0009-0002-9707-9140

3rd Marko Pap
Novelic Radar Sensors
Novelic
Belgrade, Serbia
0000-0001-9466-2774

4th Vladimir Milovanovic
Faculty of Engineering
University of Kragujevac
Kragujevac, Serbia
0000-0003-3071-4728

5th Veljko Papic
School of Electrical Engineering
University of Belgrade
Belgrade, Serbia
0000-0002-5483-7530

6th Veljko Mihajlovic
Novelic Radar Sensors
Novelic
Belgrade, Serbia
0009-0003-1771-7278

***Abstract*—Widely used in automotive safety, industrial automation, and surveillance, Frequency-Modulated Continuous-Wave (FMCW) radar provides accurate object tracking (OT). Kalman filter (KF)-based algorithms are proven to work reliably in industry for OT with FMCW radar. Extending the KF functionality, Probabilistic Data Association Filter (PDAF) is a method that also enables the association of detected reflections with the observed target. Integrated PDAF (IPDAF) offers formulations for both the probability of track existence and data association simultaneously. This paper shows how parameters for IPDAF tracker can be selected to optimize the OT. First, FMCW radar is simulated to generate precise distance, velocity, and angle measurements through a multiple-input multiple-output (MIMO) antenna setup providing ground-truth labeled data. Next, a practical method for calculating optimal tracking parameters (OTP), particularly for short-range applications, based on Optuna optimizer is introduced. This method aims to improve tracking accuracy in scenarios such as indoor environments and pedestrian safety systems, considering scenarios with different target movement maneuvers and different dynamic movement models.**

***Index Terms*—FMCW radar, radar simulation, object tracking, IPDAF, Optuna optimization**

I. Introduction

Selecting OTP for an OT is crucial as it directly impacts the accuracy and reliability of tracking results, ensuring effective monitoring across diverse scenarios. Sensors based on acoustic waves and radars offer privacy and cost-effectiveness. Human OT benefits from radar's ability to penetrate visual obstructions, making it suitable for surveillance in challenging environments. Radar-based tracking provides enhanced situational awareness in scenarios where visual conditions are poor or obstructed, such as low light, dense foliage, or adverse weather [1]. Moreover, radars are good at detecting micro motions like vital signs, which significantly increases the detectability of low Signal-to-Noise Ratio (SNR) targets [2]. Additionally, radar systems can detect multiple targets through signal modulation and MIMO systems, enhancing their versatility in tracking scenarios.

Different radar modeling approaches in the literature address specific aspects of radar systems, from environment modeling to limited building block representations [3]. However, recent radar modeling literature has shown a lack of focus on radar hardware and system modeling. This is solved in [4], where an extensive radar model is introduced. Important aspects of the radar simulation are an equivalent receiver gain and a noise figure (NF). In [5], it is shown how the NF should be interpreted generally, while [6] suggests that the receiver can be modeled with an equivalent gain and NF. For the selection of necessary parameters in this work, the TI IWR6843 radar datasheet [7] is used.

Besides radar parameters, the type of target used in the simulation influences the reflected signal significantly with its Radar Cross-Section (RCS). The focus of this paper is on simulating and tracking human targets. Pedestrian's 360 degrees radio wave reflection characteristics were measured with 76-GHz radar in [8] where it was shown that the average RCS is -8.1 dBsm with fluctuations of more than 10 dBsm. RCS for pedestrians at different angles was modeled with Weibull distribution in [9] based on 79-GHz radar measurements, while [10] additionally considers 24-GHz radar measurements with human targets in different poses and clothes. Almost linear RCS dependence on carrier frequency was reported in [11],

This work was supported by Novelic.

while moving targets' RCS was analyzed in [12].

KF is a recursive Bayesian filter suited for single-target state estimation under linear models and Gaussian noise, being at the same time one of the earliest approaches for online tracking [13]. In target-tracking applications, multidimensional gates, also called validation regions, are constructed in a measurement space to enable the association of reflections with the target of interest. Additionally, validation minimizes the need for an exhaustive search across the measurement space. PDA is a well-established technique for data association and tracking [14]. However, it assumes the existence of a track, which limits its ability to provide track existence probability information. To overcome this limitation, different approaches were introduced with a focus on track observability [15] and a combination of multiple model approach with PDA [16]. In contrast, IPDA redefines PDA without assuming track existence initially [17] offering expressions for both track existence probability and data association simultaneously. IPDA maintains computational efficiency like PDA while achieving better performance.

The purpose of our research is to determine the OTP of the IPDAF tracker for people tracking. It is shown how the received radar reflection can be modeled with a few parameters for the radar components, signal propagation through the environment, and targets. To obtain relevant optimization results, trajectories of the target's movement were simulated in different ways to cover all demanding situations for tracking people with radars known from practice. A loss function for one set of parameters is defined as the mean loss for all trajectories and based on the loss, Optuna optimizer [18] is run to select OTP.

II. Radar simulation

The basic principle of FMCW radar involves transmitting a signal with a frequency that linearly increases or decreases over time (chirp) [19]. When this signal encounters an object, a portion of the energy is reflected to the radar receiver. By comparing the frequency of the transmitted signal with the frequency of the received signal, the radar can determine the range (r) of the object. Radial velocity (v) information can be extracted by transmitting multiple chirps closely separated in time [19]. Modern FMCW radars utilize MIMO antenna arrays to enable Angle of Arrival (AOA) estimation of the detected targets, including azimuth (ϕ) and elevation (θ) angles. Therefore, each detected target is described by four directly measured parameters $\langle r, v, \phi, \theta \rangle$. Extending the vector with the SNR and forming a list of all detected targets results in a radar point cloud (PC).

To circumvent the need for simulating radar signals at high frequencies and individually modeling components within the transmitting and receiving radar chains, the simulation focuses on generating received baseband signals. This involves defining simulation parameters encompassing radar configuration, radar parameters, and target characteristics, specifically tailored for detecting moving human targets within a 10-meter range. The radar configuration, including transmitter and receiver parameters, is detailed, while the target's movement trajectory is determined based on the initial position, speed, and acceleration profile.

A. Radar configuration and parameters

Using the Time-Division Multiplexing (TDM) technique [20], the simulation facilitated signal separation from different transmitting (TX) antennas by the receiving (RX) antennas. The selection of radar configuration parameters is contingent upon factors such as the target type, expected dynamics, environmental conditions, and the designated detection zone. Target dynamics significantly influence parameters governing maximum achievable speed and speed resolution. Specifically, the maximum speed of the target is inversely proportional to the time interval between successive chirps emitted by the same TX antenna, while increasing the number of chirps per antenna improves speed resolution. Additionally, the detection zone dictates the maximum target distance, which, in turn, influences the choice of Analog-to-Digital Converter (ADC) selection frequency, with the maximum distance proportional to the frequency component post-range Fast Fourier Transform (FFT). In this simulation, a complex sampling mode labeled "complex1" was employed, as defined in the TI documentation [21]. Furthermore, the chirp bandwidth determines distance measurement resolution. Key radar configuration parameters can be summarized as: central frequency $F_c = 60\text{GHz}$, total chirping time $T_c = 50.5\mu\text{s}$, total idle time $T_{idle} = 7\mu\text{s}$, total bandwidth $BW = 3.099\text{GHz}$, number of TX channels $N_{TX} = 3$, number of RX channels $N_{RX} = 4$, number of chirps $N_c = 32$, number of ADC samples per chirp $N_{adc} = 256$ and sampling frequency $F_s = 5.9\text{MHz}$.

The radar is approximated with a few parameters to obtain realistic SNR values of observed targets to simplify the analysis. A sufficient set of parameters includes gains of the transmitting G_t and receiving antennas G_r and the equivalent characteristics of the receiving chain, which is represented as a black box and defined by three parameters: equivalent gain ($G_e = 36\text{dB}$), NF ($F = 12\text{dB}$) and bandwidth ($B_e = 5.9\text{MHz}$). G_t and G_r are both given with (1) for $\theta \in [-90°, 90°]$, where $G_{max} = 12\text{dB}$.

$$\begin{aligned} G(\theta) &\sim \mathcal{N}(20\log_{10}(\cos(0.01309\theta) + 0.01), 0.09) \\ G_t(\theta) &= G_r(\theta) = G_{\max} + G(\theta) - \max_{\theta}(G(\theta)). \end{aligned} \tag{1}$$

The equivalent model of the receiving chain is excited by the received useful signal, which represents the reflection of the transmitted signal from the target, and thermal noise of spectral density kT, where k is the Boltzmann constant and T is the temperature at the receiver input in Kelvin. A nominal value of $290\,\text{K}$ is chosen for T. The model of the receiving chain introduces additional noise into the system, which is modeled by the degradation of the input SNR and modeled by NF. Therefore, the output noise power of the receiver chain model is equal to the sum of the input thermal noise propagation contribution and the model's noise, assuming that they are uncorrelated.

On the other hand, the NF can be seen as a value by which the input spectral density of the thermal noise power kT should be multiplied to produce the output noise equal to the sum of the propagated and intrinsic noise after propagation through the noiseless receiving chain. Thus, the spectral noise power density at the input becomes kTF, while the output thermal noise power is equal to $kTFB_eG_e$ [10, 11]. A useful signal is also propagated through the receiver chain model. Considering that the frequency components of the useful signal are within the receiver's bandwidth B_e, the useful signal is affected only by the gain G_e. Provided that the antenna and receiver impedance are ideally matched and equal to $50\,\Omega$, the signal and noise output peak-to-peak values can be estimated from the receiver chain model as:

$$V_{\text{spp}} = \sqrt{2 \cdot 4 \cdot P_{\text{S}} R} 10^{\frac{G_{\text{e}}}{20}}, \tag{2}$$

$$V_{\text{npp}} = \sqrt{2 \cdot 4 \cdot kTF_{\text{e}} B_{\text{e}} R} 10^{\frac{G_{\text{e}}}{20}}, \tag{3}$$

where V_{spp} is the output peak to peak signal value, V_{npp} is the output peak to peak noise value, P_s is the input signal power given by the radar equation (4).

B. Targets in the radar environment

In the context of short-range radar systems designed for pedestrian detection, the operating environment comprises both stationary clutter, such as urban infrastructure and natural elements, alongside dynamic entities like pedestrians, pets, cyclists, and vehicles. Radar waves, upon transmission, interact with these surroundings, reflecting off objects and returning to the radar's receiver. The radar equation (4) is used to calculate the power of the received signal in radar systems, helping determine the effectiveness of the radar in detecting targets against background clutter and noise. This equation accounts for parameters including transmitted signal power P_t, antenna gains (G_t and G_r), wavelength (λ), radar cross-section (σ), and target range (R), ultimately determining the power of the received signal (P_r) at the radar's receiver antenna [22]. Additional environmental losses are neglected.

$$P_r = \frac{P_t G_t G_r \lambda^2 \sigma}{(4\pi)^3 R^4}. \tag{4}$$

In (4), the reflected signal power is directly proportional to a target's RCS. The target of interest in the simulation is a pedestrian. The wavelength of the simulated radar is small compared to the target's dimension. This complex target can be seen as a collection of individual reflecting scatterers [22]. Viewing aspect of the target can vary over time as the target is moving. Even small changes in the viewing aspect can result in huge RCS variations. Using the results from [8], RCS of the target is modeled according to:

$$RCS \sim \mathcal{N}(-8, 16) \tag{5}$$

OTP are estimated for moving targets in the radar environment. The simulation sampling period (Δt) is equal to the duration of one radar frame, which is 80 ms. This is a relatively short time interval for a significant change in the dynamics of the human target's movement. Accordingly, a simulation of the target's trajectory was performed based on the parameters of the trajectory profile: initial position $\langle x_0, y_0 \rangle$, initial velocity $\langle v_{\text{x}0}, v_{\text{y}0} \rangle$, acceleration profile $\langle a_{\text{x}}(t), a_{\text{y}}(t) \rangle$ and simulation time Δt, as follows:

$$\begin{aligned} v_x(t) &= v_x(t-1) + a_x(t-1)\Delta t \\ v_y(t) &= v_y(t-1) + a_y(t-1)\Delta t \\ x(t) &= x(t-1) + v_x(t)\Delta t \\ y(t) &= y(t-1) + v_y(t)\Delta t. \end{aligned} \tag{6}$$

III. Optimal tracking parameters

This chapter explains the tracking procedure used for a target state estimation in the presence of clutter and the optimization method for selecting the OPT.

A. IPDA tracker

PDAF is a practical estimator that includes data association for one target in the presence of clutter. This estimator is based on the minimum mean square error (MMSE) approach and estimates the conditional probability distribution of the target state in each estimation step. PDA algorithm computes association probabilities between validated measurements and the target being tracked, incorporating Bayesian information to handle measurement origin uncertainty. It utilizes a KF for linear state and measurement equations, transitioning to an Extended KF (EKF) when equations are nonlinear in the PDAF tracking algorithm [14].

Starting from the assumption that only one target is present in the zone of interest, the evolution of the system state in time can be approximated by

$$x(k) = F(k-1)x(k-1) + v(k-1), \tag{7}$$

where the measurements coming from the target are described with

$$z(k) = H(k)x(k) + w(k). \tag{8}$$

In the equations (7) and (8), $v(k-1)$ and $w(k)$ are zero-mean mutually independent, white Gaussian noise sequences described with known covariance matrices $Q(k-1)$ and $R(k)$. It is further assumed that the track has been initialized. Gaussian posterior is used to describe the past information about the target. In each tracking step, a validation region is set in the measurement space around the predicted measurement. The candidate measurements are selected and if the target was detected with a probability of detection P_D, then only one of the gated measurements can originate from the target. The remaining reflections are assumed to be independent and identically distributed with uniform spatial distribution [14]. The PDA principle is a basis for estimation algorithms that additionally include modeling of the track existence.

IPDA used for OT based on the simulated reflections from the targets models the existence of a track using a Markov process, relating the probability of the target's existence at

time k to the probability that the target does not exist at the same time as follows [17]:

$$\begin{aligned} P(x_k) &= p_{11}P(x_{k-1}) + p_{21}(1 - P(x_{k-1})) \\ 1 - P(x_k) &= p_{12}P(x_{k-1}) + p_{22}(1 - P(x_{k-1})), \end{aligned} \tag{9}$$

where $P(x_k)$ represents the probability of track existence at scan k while probability that the track does not exist at scan k is modeled as $1 - P(x_k)$.

The coefficients describing the probabilities of transition from state to state of the model satisfy the rule:

$$p_{11} + p_{12} = p_{21} + p_{22}. \tag{10}$$

In [17], it is further shown that starting from modeling the existence of the target, following the steps of prediction, association, and estimation, the same formulas that apply to the original PDAF filter [14] are reached. Fig. 1 shows the steps with the corresponding formulas for IPDA tracker based on the Markov chain defined in (9).

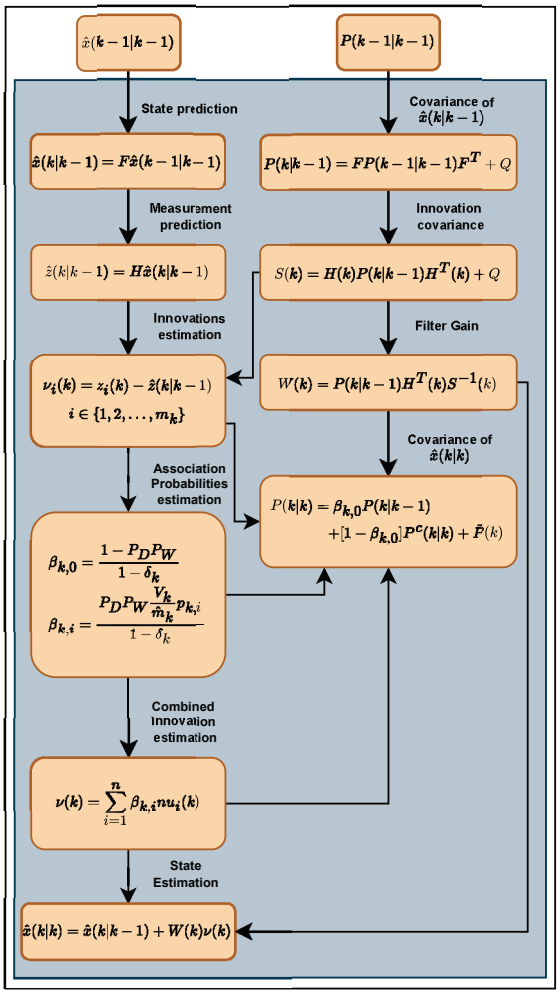

Fig. 1: One cycle of the IPDA filter.

At radar scan k, the matrix $H(k)$ is defined in (11) and the rest of the expressions from Fig. 1 can be found in [17].

$$\begin{aligned} H(k) &= \left.\frac{\partial h}{\partial x}\right|_{x(t|t-1)} \\ h(x,y) &= \begin{bmatrix} \sqrt{\mathrm{x}^2 + \mathrm{y}^2} \\ \tan^{-1}(\mathrm{x},\mathrm{y}) \\ \frac{\mathrm{x}\dot{y} + \mathrm{y}\dot{y}}{\sqrt{\mathrm{x}^2+\mathrm{y}^2}} \end{bmatrix} \end{aligned} \tag{11}$$

B. *Optuna optimizer*

Optuna is a next-generation hyperparameter optimization framework that employs a ”define-by-run” methodology [18]. This approach, along with a Tree-structured Parzen Estimator (TPE) is a significant development in Bayesian optimization techniques [23]. It allows dynamic definition and adjustment of hyperparameters during runtime, which contrasts traditional static configurations. This flexibility is crucial for complex models, where OTP may be identified based on intermediate feedback during the model's performance.

In Optuna, the process of evaluating different sets of hyperparameters is organized into ”trials” and ”studies”. Each trial tests a specific set of hyperparameters within the defined search space and is assessed by an objective function that is defined to maximize or minimize its output. A study includes multiple trials to determine the optimal hyperparameters that maximize the performance of the objective function. Additionally, Optuna incorporates advanced pruning mechanisms like the Asynchronous Successive Halving Algorithm (ASHA), which allocates minimal initial resources to each trial and prunes less promising ones based on performance metrics at designated checkpoints, optimizing resource use [24].

IV. Radar Simulation and Tracking Results

Before starting the Optuna optimizer to obtain the OTP of the IPDAF tracker, it is necessary to simulate the target's movement in the area of interest (AOI). Parameters of the radar, signal propagation through the environment, and target are presented in the previous chapters. Based on these parameters and profiles of trajectories of the target's movement, optimization data is collected for each radar frame in the form of a PC and corresponding ground truth positions. The PC originates from a conventional radar processing pipeline depicted in Fig. 2.

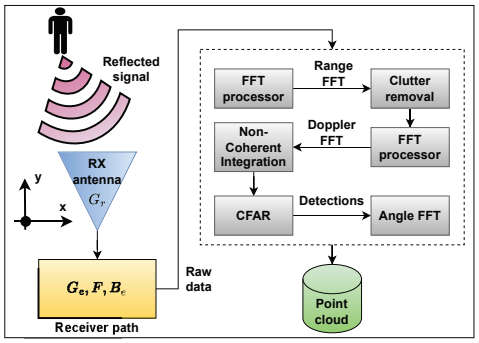

Fig. 2: Radar processing pipeline used for generating the PC.

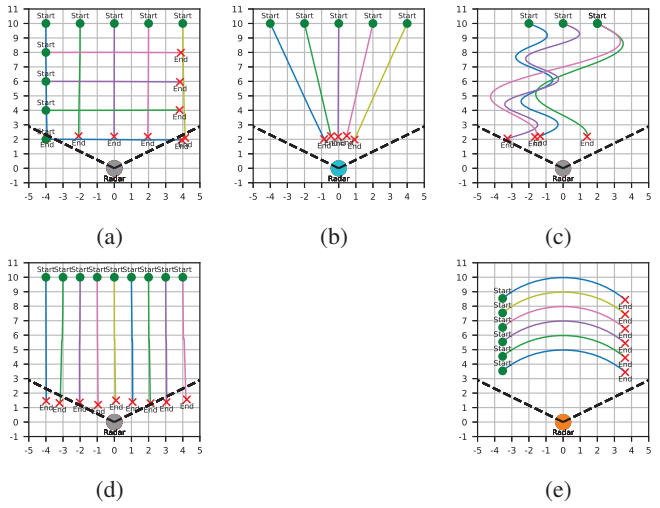

Fig. 3: Examples of different trajectories used for generating optimization data.

The FFT is applied to the received chirps to determine the range of detected objects (Range FFT). The next step involves static clutter removal, which eliminates reflections from the non-moving objects in the environment. Again, FFT is used to estimate the velocity of the detected objects by applying FFT across chirps. Non-coherent summation of Doppler FFT results in a Doppler map. The Doppler map is an input to the detection block based on the two-stage Constant False Alarm Rate (CFAR) [22] algorithm. Two-stage CFAR utilizes two standard CFAR detectors: one for rows and one for columns of the Doppler map. A third FFT is used to estimate the angle of arrival of the detected points. SNR is estimated as a ratio of signal amplitude and noise level estimated in the CFAR. The resulting array of points represents the PC.

In addition to multiple possible reflections from the target, the PC can also contain reflections from clutter. Clutter is evenly spread throughout the observation region and its quantity follows a Poisson distribution pattern with a spatial density of $\lambda = 0.02$ clutter points per square meter. Clutter is not added directly to the PC, but is also simulated as a radar reflection from a certain number of interfering targets with the SNR high enough to pass the detection threshold of CFAR.

Achieving valid optimization results hinges on the quality of the collected data, which is influenced by both the movement patterns of the target and the amount of clutter in the AOI. Therefore, great attention is paid to the variety of target motion and includes the following situations: (a) straight-line motion at constant speed horizontally and vertically, (b) straight-line motion at constant speed radially toward the radar, (c) motion at constant speed with random turns, (d) motion with random stopping, (e) moving along a circular trajectory. Cases (a)-(e) are shown in Fig. 3. The total number of generated trajectories (N_t) is 35.

Tracking parameters are optimized using a loss function that measures the mean Euclidean distance between the estimated target state and the ground truth position. Let $N(k)$ be the total number of frames in k-th trajectory. Starting from the mean square error (MSE) for a k-th trajectory (12),

$$MSE(k) = \frac{1}{N_c(k)} \sum_{i=1}^{N_c(k)} |\hat{x}^{(i)} - x_{gt}^{(i)}|^2, \tag{12}$$

where $N_c(k)$ is the number of frames in which the track was confirmed, $\hat{x}^{(i)}$ is the state estimation in the i-th frame, and $x_{gt}^{(i)}$ is the ground truth position in the i-th frame, the loss function for a single trajectory (13) is defined as the ratio of $MSE(k)$ and $N_c(k)$. Thus, the loss defined in (12) is further reduced by the number of frames with the confirmed track.

$$\mathtt{L}(k) = \frac{1}{N_c(k)} MSE(k). \tag{13}$$

The overall loss (14) is defined as the mean value of losses for the entire set of trajectories.

$$\mathtt{L}_t = \frac{1}{N_t} \sum_{i=1}^{N_t} \mathtt{L}(k) \tag{14}$$

Consider a nearly constant velocity (CV) or constant acceleration (CA) model in two dimensions with the following parameters:

$$\begin{aligned}
&\mathbf{Q_{cv}} = \mathbf{Q_{cv,0}} \cdot q_{\text{coeff}}, \\
&\mathbf{Q_{ca}} = \mathbf{Q_{ca,0}} \cdot q_{\text{coeff}}, \\
&\mathbf{R} = \mathbf{R_{cv}} = \mathbf{R_{ca}} = diag(r_{11}^2, r_{22}^2, r_{33}^2) \\
&\mathbf{P_{cv}}(\mathbf{0}|\mathbf{0}) = diag(p_{0,00}^2, p_{0,11}^2, p_{0,22}^2, p_{0,33}^2) \\
&\mathbf{P_{ca}}(\mathbf{0}|\mathbf{0}) = diag(p_{0,00}^2, p_{0,11}^2, p_{0,22}^2, p_{0,33}^2, p_{0,44}^2, p_{0,55}^2),
\end{aligned} \tag{15}$$

where T is equal to the radar frame cycle and $diag$ is the notion for a diagonal matrix with all elements equal to zero except the ones on the main diagonal provided in brackets. Next, $\mathbf{Q_{cv}}$ and $\mathbf{Q_{ca}}$ are process noise covariances for CV and CA respectively, $\mathbf{Q_{cv,0}}$ and $\mathbf{Q_{ca,0}}$ are derived from the direct discrete-time kinematic model [17], $\mathbf{P_{cv}}(\mathbf{0}|\mathbf{0})$ and $\mathbf{P_{ca}}(\mathbf{0}|\mathbf{0})$ are initial state covariances for CV and CA respectively, while $\mathbf{R}$ is the measurement covariance. The rest of parameters from (15) are optimized together with coefficients from the Markov model (9), detection probability P_D [14], and the initial probability of track existence P_{te}. The space in which parameters are optimized is defined with $q_{\text{coeff}} \in [0.1, 30]$, $r_{11} \in [0.01, 0.5]$, $r_{22} \in [0.01, 0.2]$, $r_{33} \in [0.1, 3]$, $p_{0,00} \in [0.1, 10]$, $p_{0,11} \in [0.1, 10]$, $p_{0,22} \in [0.01, 10]$, $p_{0,33} \in [0.01, 10]$, $p_{0,44} \in [0.001, 10]$, $p_{0,55} \in [0.001, 10]$, $P_D \in [0.8, 0.99]$, $P_{te} \in [0.2, 1]$, $p_{11} \in [0.7, 1]$, $p_{21} \in [0, 0.4]$.

Optimization was conducted for both CV and CA target motion models. Table I summarizes the mean losses for each trajectory class, as well as the total mean loss for each model. Given mean losses values should be divided by 1000 to reach the original values. The results indicate that employing a simple CV model suffices for tracking individual targets in clutter without sacrificing performance. This conclusion is

supported by Fig. 4, which illustrates the tracking results of reference positions for both CV and CA models.

TABLE I: Mean losses for each trajectory class and the total mean loss for each model.

	Trajectories					
	A	B	C	D	E	Total
CV	1.279	1.639	1.142	0.729	0.476	1.021
CA	1.283	1.791	1.180	0.709	0.488	1.046

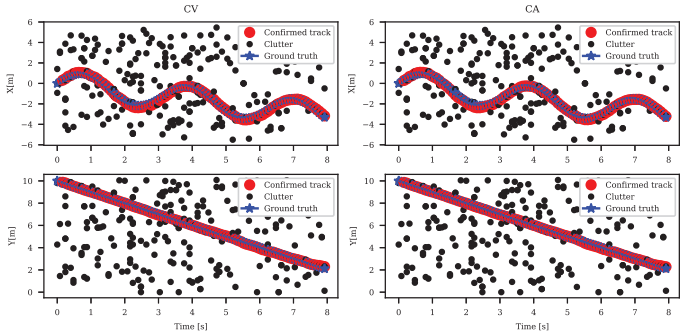

Fig. 4: Tracking results for the selected optimal parameters for maneuvering targets.

V. Conclusion

This paper investigates the selection of OTP for human tracking by utilizing the Optuna optimizer. The loss function for the complete optimization dataset was defined as a mean value of individual losses for each trajectory. The dataset was collected in the FMCW radar simulation, which modeled the radar with its transmitter and receiver parameters. Propagation of the signal through the environment was modeled with the radar equation not considering radar losses due to the small detection zone. Human target trajectories were created to cover challenging tracking scenarios for the radar. IPDAF tracker was selected for OT since it consists of a fully integrated method for track initiation, data association, and track smoothing. Following optimization and the application of a basic CV model, our system robustly achieves diverse maneuver objectives in cluttered environments, demonstrating its effectiveness.

VI. Acknowledgment

We would like to express our sincere gratitude to Professor Zoran Popovic for his invaluable guidance and feedback. Additionally, we extend our heartfelt thanks to Novelic for generously financing our participation in the conference.

References

[1] Q. Chen, Y. Xie, S. Guo, J. Bai, and Q. Shu, "Sensing system of environmental perception technologies for driverless vehicle: A review of state of the art and challenges," *Sensors and Actuators A: Physical*, vol. 319, p. 112566, 2021.

[2] S. Marty, A. Ronco, F. Pantanella, K. Dheman, and M. Magno, "Frequency Matters: Comparative Analysis of Low-Power FMCW Radars for Vital Sign Monitoring," *IEEE Transactions on Instrumentation and Measurement*, vol. 73, pp. 1–10, 2024.

[3] M. Brooker and M. Inggs, "A Signal Level Simulator for Multistatic and Netted Radar Systems," *IEEE Transactions on Aerospace and Electronic Systems*, vol. 47, no. 1, pp. 178–186, 2011.

[4] J. Kannanthara, D. Griffiths, M. Jahangir, J. M. Jones, C. J. Baker, M. Antoniou, C. J. Bell, H. White, K. Bongs, and Y. Singh, "Whole system radar modelling: Simulation and validation," *IET Radar, Sonar & Navigation*, vol. 17, no. 6, pp. 1050–1060, 2023.

[5] A. W. Doerry, "Noise and noise figure for radar receivers," Sep 2016.

[6] Y. Wu and J. Linnartz, "Detection performance improvement of fmcw radar using frequency shift," in *Proceedings of the 32nd WIC Symposium on Information Theory in the Benelux, 10-11 May 2011, Brussels, Belgium*, pp. 1–8, Université Libre de Bruxelles, 2011.

[7] T. Instruments, "Iwr6843, iwr6443 single-chip 60- to 64-ghz mmwave sensor," Tech. Rep. SWRS219E, Texas Instruments Incorporated, 2018. Datasheet.

[8] N. Yamada, Y. Tanaka, and K. Nishikawa, "Radar cross section for pedestrian in 76GHz band," in *2005 European Microwave Conference*, vol. 2, pp. 4 pp.–1018, 2005.

[9] M. Yasugi, Y. Cao, K. Kobayashi, T. Morita, T. Kishigami, and Y. Nakagawa, "79GHz-band radar cross section measurement for pedestrian detection," in *2013 Asia-Pacific Microwave Conference Proceedings (APMC)*, pp. 576–578, 2013.

[10] J. R. Centre, I. for the Protection, S. of the Citizen, J. Chareau, and J. Fortuny-Guasch, *Radar cross section measurements of pedestrian dummies and humans in the 24/77 GHz frequency bands - Establishment of a reference library of RCS signatures of pedestrian dummies in the automotive radar bands*. Publications Office, 2013.

[11] T. Motomura, K. Uchiyama, and A. Kajiwara, "Measurement results of vehicular RCS characteristics for 79GHz millimeter band," in *2018 IEEE Topical Conference on Wireless Sensors and Sensor Networks (WiSNet)*, pp. 103–106, 2018.

[12] Y. Deep, P. Held, S. S. Ram, D. Steinhauser, A. Gupta, F. Gruson, A. Koch, and A. Roy, "Radar cross-sections of pedestrians at automotive radar frequencies using ray tracing and point scatterer modelling," *IET Radar, Sonar & Navigation*, vol. 14, pp. 833–844, 2020.

[13] R. E. Kalman, "A New Approach to Linear Filtering and Prediction Problems," *Journal of Basic Engineering*, vol. 82, pp. 35–45, 03 1960.

[14] Y. Bar-Shalom, F. Daum, and J. Huang, "The probabilistic data association filter," *IEEE Control Systems Magazine*, vol. 29, no. 6, pp. 82–100, 2009.

[15] S. Colegrove and S. Davey, "On using nearest neighbours with the probabilistic data association filter," in *Record of the IEEE 2000 International Radar Conference [Cat. No. 00CH37037]*, pp. 53–58, 2000.

[16] A. Houles and Y. Bar-Shalom, "Multisensor tracking of a maneuvering target in clutter," *IEEE Transactions on Aerospace and Electronic Systems*, vol. 25, no. 2, pp. 176–189, 1989.

[17] D. Musicki, R. Evans, and S. Stankovic, "Integrated probabilistic data association," *IEEE Transactions on Automatic Control*, vol. 39, no. 6, pp. 1237–1241, 1994.

[18] T. Akiba, S. Sano, T. Yanase, T. Ohta, and M. Koyama, "Optuna: A Next-generation Hyperparameter Optimization Framework," in *Proceedings of the 25th ACM SIGKDD International Conference on Knowledge Discovery & Data Mining*, KDD '19, (New York, NY, USA), pp. 2623–2631, Association for Computing Machinery, 2019.

[19] G. Brooker, "Understanding millimetre wave FMCW radars," in *1st international Conference on Sensing Technology*, vol. 1, 2005.

[20] S. Hamidi, M.-R. Nezhad-Ahmadi, and S. Safavi-Naeini, "TDM based Virtual FMCW MIMO Radar Imaging at 79GHz," in *2018 18th International Symposium on Antenna Technology and Applied Electromagnetics (ANTEM)*, pp. 1–2, 2018.

[21] K. Ramasubramanian, "Using a complex-baseband architecture in FMCW radar systems," Tech. Rep. SPYY007, Texas Instruments, 2017. Whitepaper.

[22] M. I. Skolnik, *Introduction to radar systems*. Boston: Mcgraw-Hill, 2007.

[23] S. Watanabe, "Tree-structured parzen estimator: Understanding its algorithm components and their roles for better empirical performance," *ArXiv*, vol. abs/2304.11127, 2023.

[24] L. Li, K. G. Jamieson, A. Rostamizadeh, E. Gonina, J. Ben-tzur, M. Hardt, B. Recht, and A. Talwalkar, "A system for massively parallel hyperparameter tuning," *arXiv: Learning*, 2018.